Electronic Supplementary Material (ESI) for Materials Chemistry Frontiers.

Supporting Information

In situ reconstruction of vegetable sponge-like Bi_2O_3 for efficient CO_2 electroreduction to formate

Yingli Shi, Chun Fang Wen, Xuefeng Wu, Jia Yue Zhao, Fangxin Mao, Peng Fei Liu, Hua Gui Yang**

Key Laboratory for Ultrafine Materials of Ministry of Education, Shanghai Engineering Research Center of Hierarchical Nanomaterials, School of Materials Science and Engineering, East China University of Science and Technology. 130 Meilong Road, Shanghai 200237, China.

Email: hgyang@ecust.edu.cn, fxmao@ecust.edu.cn.

Experimental section

Chemicals

Bismuth(III) nitrate pentahydrate ($Bi(NO_3)_3•5H_2O$) and hydrochloric acid (HCl, 36.0~38.0%) was purchased from Sinopharm Chemical reagent Co., Ltd. Dicyandiamide (DCD) was obtained from Alfa Aesar. Ethylene glycol (EG), Potassium hydroxide and acetone were from Yonghua Chemical Co., Ltd. Ethanol was bought from Shanghai Titan Scientific Co., Ltd. Sustainion^{TM} XA-9 (5% in ethanol) was obtained from Dioxide Materials. All chemicals were of analytical grade and used without any further purification. Deionized (DI) water used in our experiments was supplied by Milli-Q System (Millipore, Billerica, MA).

Electrochemical measurements

We used the three-electrode system flow cell setup to carry out the CO_2RR processes, among which the three electrodes refer to the working electrode, reference electrode and counter electrode. The counter electrode is a piece of pretreated nickel foam with area of 3*3 cm^2. Typical pretreatment procedure is that ultrasonic washing with 3 M HCl, acetone, ethanol and deionized water for 15 min in sequence and followed by drying in the vacuum oven.

Faradaic efficiency calculations

The Faradaic efficiency (FE) for formation of CO or H_2 was calculated as below:

$$FE = \frac{2\chi \times p \times G \times F}{I \times R \times T}$$

χ (vol%) is the volume fractions of CO or H_2, I (A) is the steady-state total current, G = 20 sccm is the flow rate of CO_2, p = 1.013×10^5 Pa, T = 293.15 K, F = 96485 C

mol^{-1}, R = 8.3145 J mol^{-1} K^{-1}.

Liquid product of $HCOO^-$ was quantified using ^1H nuclear magnetic resonance (NMR). The Faradaic efficiency for formation of $HCOO^-$ was calculated as the following:

$$FE = \frac{2F \times n_{HCOO^-}}{I \times t}$$

n_{HCOO-} (mol) is measured quantity of $HCOO^-$ and t (s) is electrolytic time.

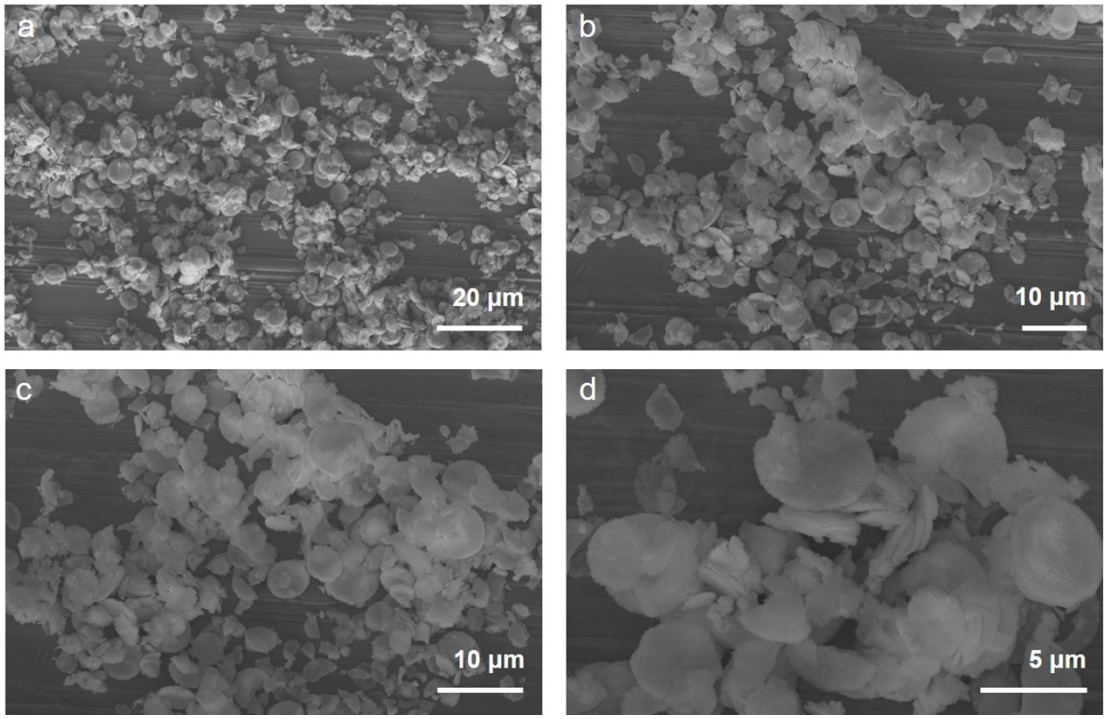

Figure S1 SEM images of VS-Bi_2O_3, showing the large-scale morphology.

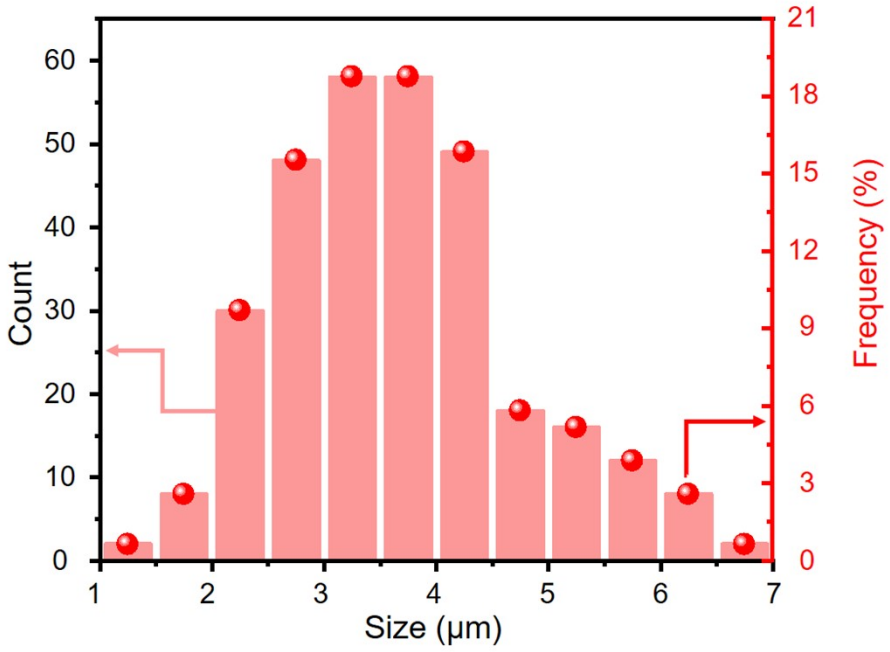

Figure S2 Size distribution statistics of VS-Bi_2O_3 (conducted based on the SEM image of Figure S1a) with main size about 3-4 μm.

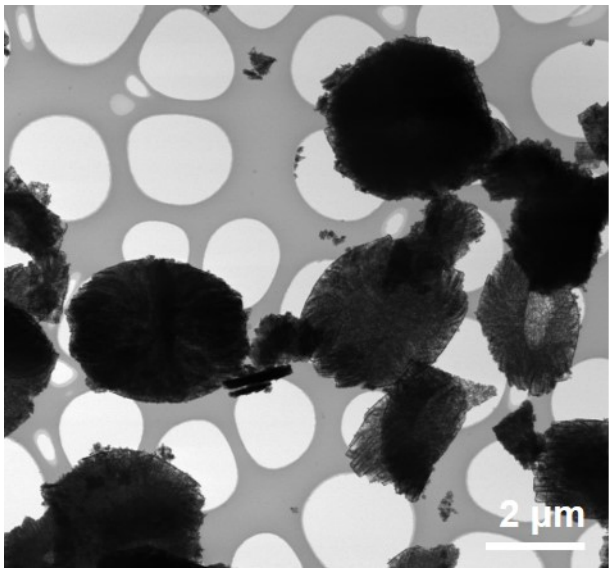

Figure S3 Low-resolution TEM image of VS-Bi_2O_3, showing its porous vegetable sponge-like morphology.

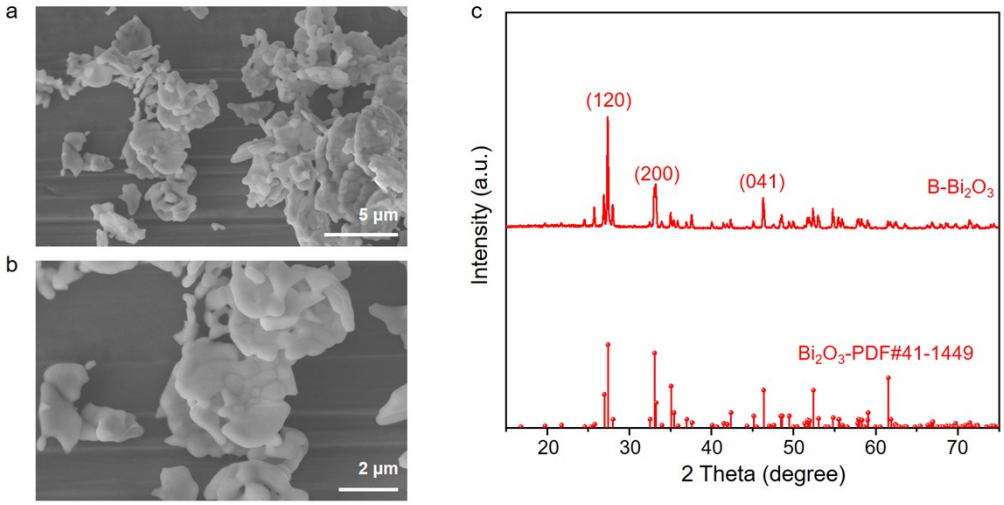

Figure S4 (a, b) SEM images of B-Bi_2O_3, showing smoother surface than the VS-Bi_2O_3 sample. (c) XRD pattern of B-Bi_2O_3 in line with monoclinic Bi_2O_3-PDF#41-1449.

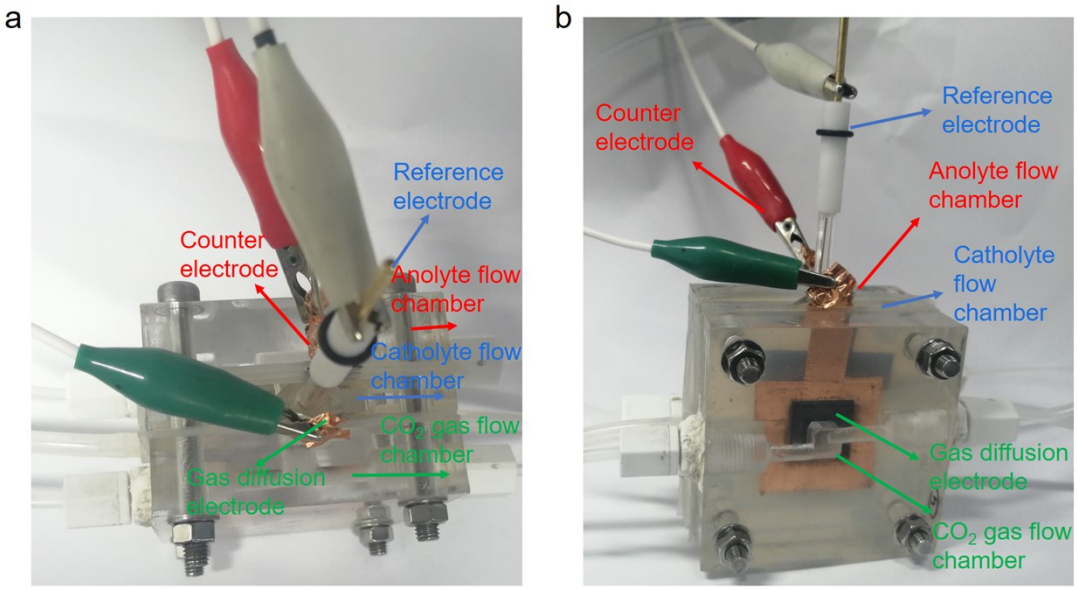

Figure S5 Flow cell setup. In the three-electrode setup, the Ag/AgCl electrode was applied as the reference electrodes, and the pretreated nickel foam was used as counter electrode, also known as anode, for the anodic oxygen evolution reaction. The flow cell design provides a gas-liquid-solid triple phase boundary, which serves as the spot where CO_2 reduction reaction carries out.

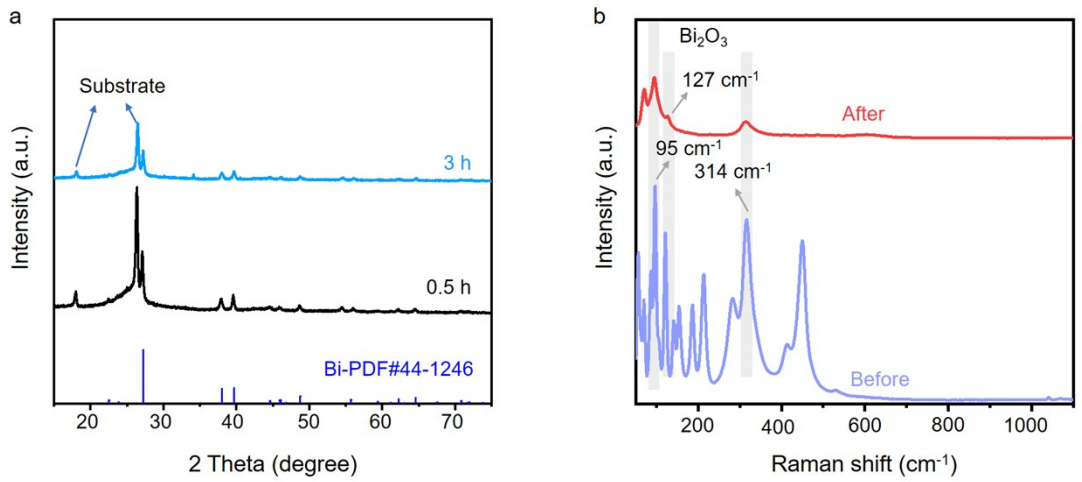

Figure S6 (a) XRD patterns of post-electrolysis (for 0.5 and 3 h, respectively) of B-Bi_2O_3, well indexed to metallic bismuth (Note that the substrate is GDE). (b) Raman spectra of B-Bi_2O_3 before reaction (blue line) and after reaction (red line) for 3 h, both of which show the existence of Bi_2O_3 (light grey shadow) without $Bi_2O_2CO_3$ detected. Figure S6a, b indicate the lack of $Bi_2O_2CO_3$ for B-Bi_2O_3 under the CO_2RR process.

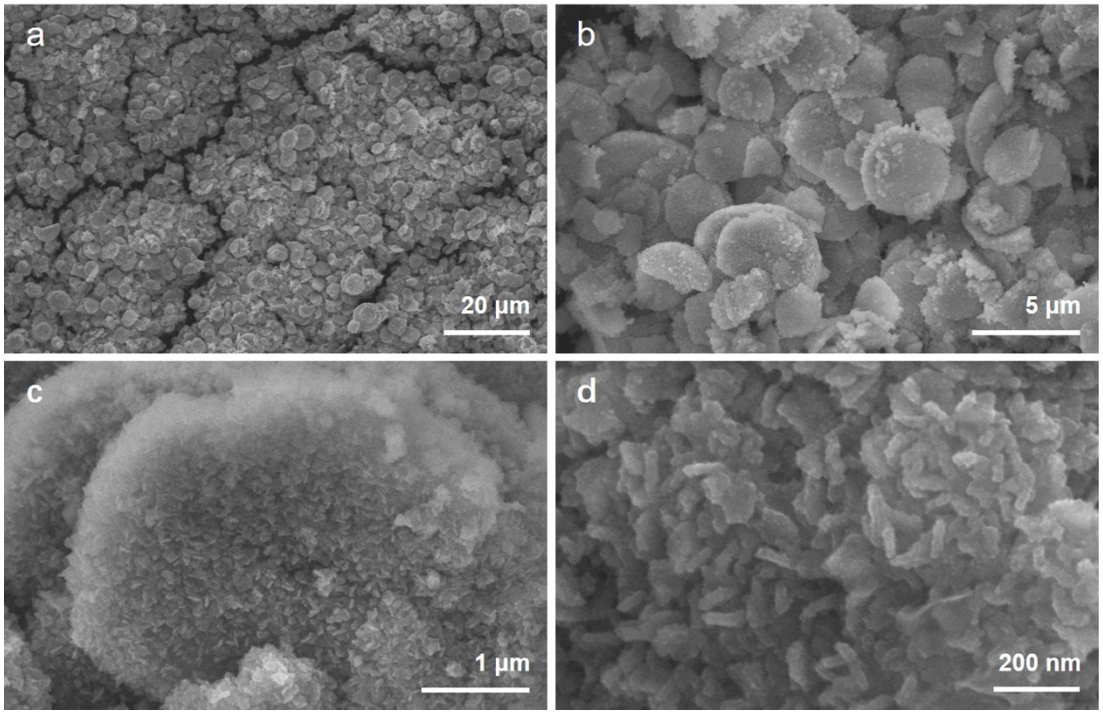

Figure S7 SEM images of post-electrolysis (for 3 h) sample of VS-Bi_2O_3, showing the thick nanoplate-assembled morphology.

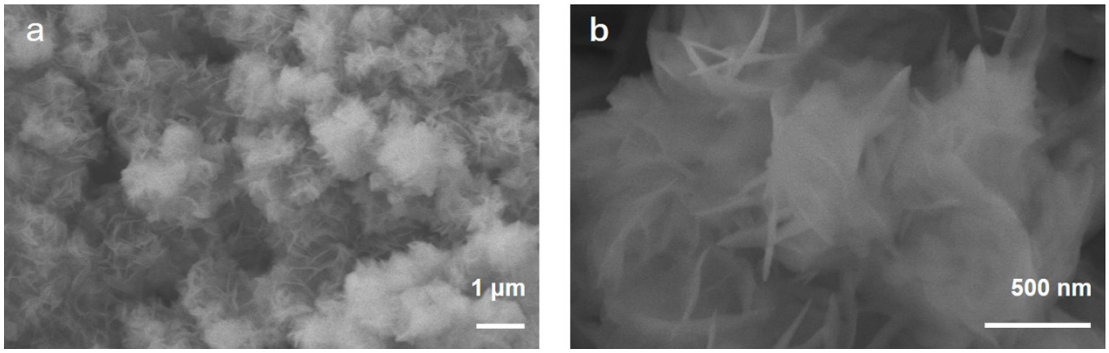

Figure S8 SEM images of post-electrolysis (for 10 h) sample of VS-Bi_2O_3, showing the nanosheets morphology.

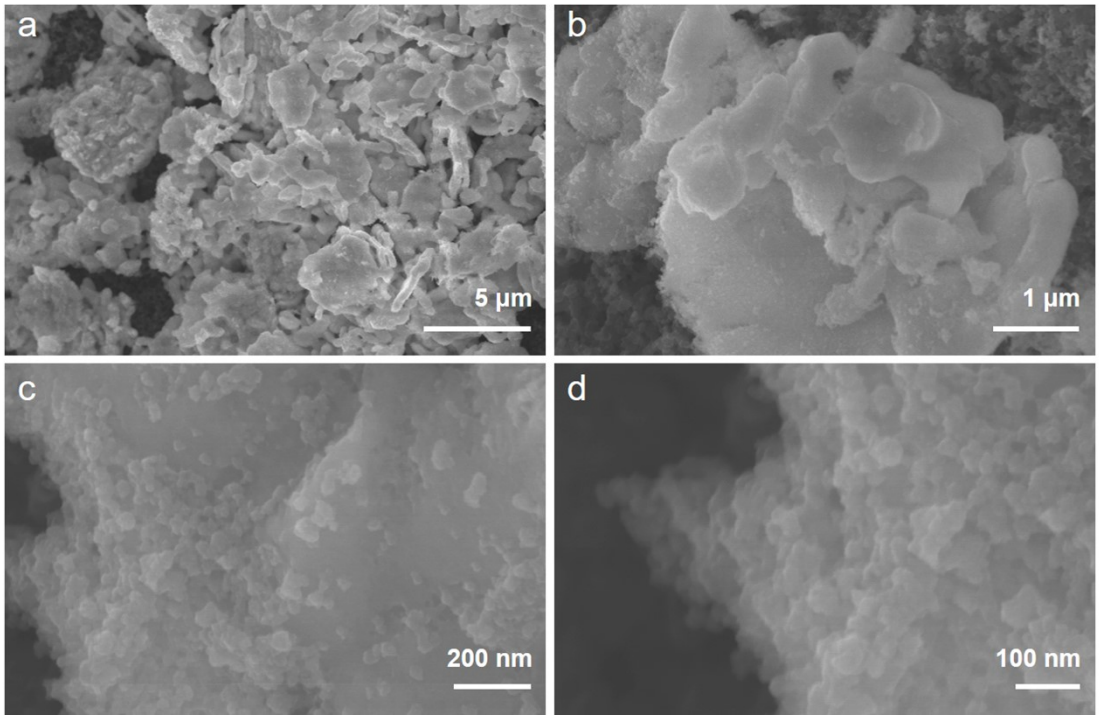

Figure S9 SEM images of post-electrolysis (for 0.5 h) sample of B-Bi_2O_3.

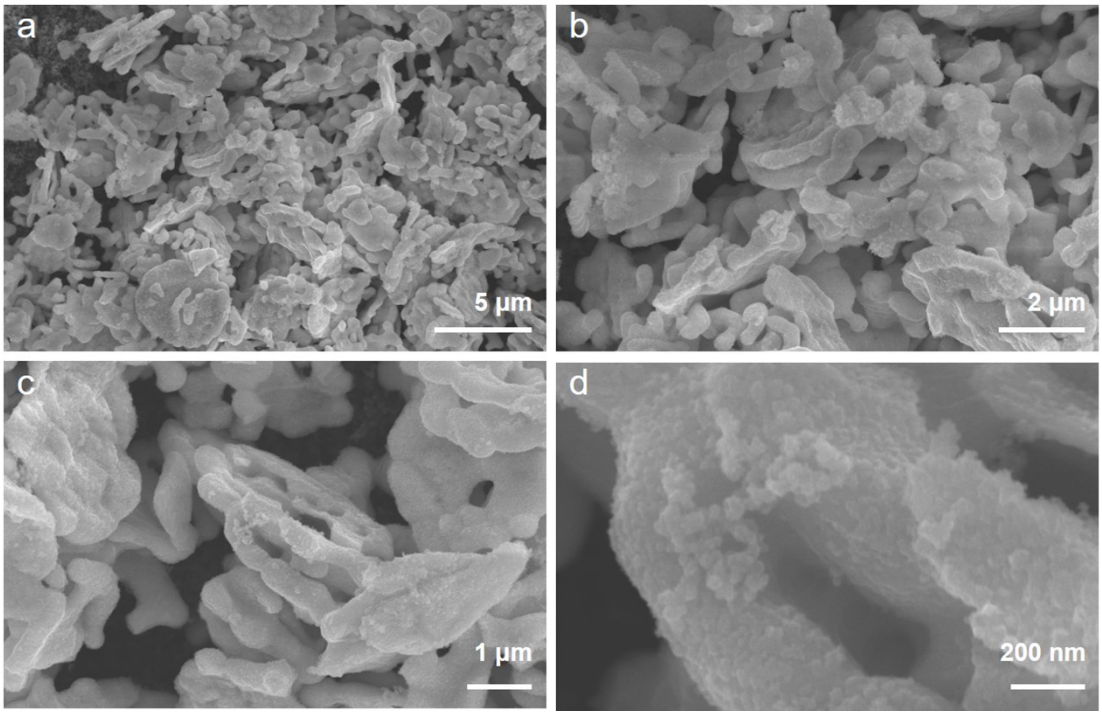

Figure S10 SEM images of post-electrolysis (for 3 h) sample of B-Bi_2O_3.

Table S1 Conditions of three different samples. All samples were assembled in the flow cell setup and lasted for 30 min, whose electrolyte was 1 M KOH.

Line color	**black**	**blue**	**red**
Gas	Ar	CO_2	CO_2
Applied current density (mA cm^{-2})	0	0	100

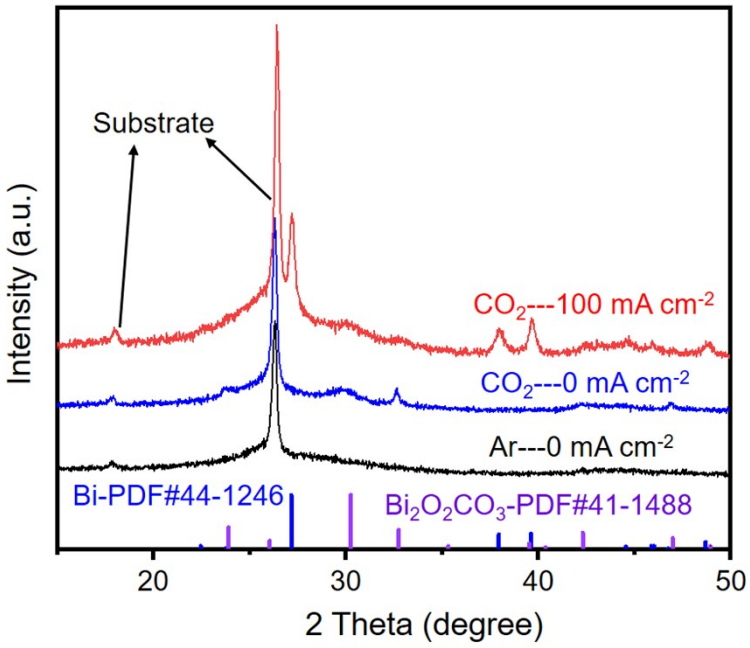

Figure S11 XRD patterns of VS-Bi_2O_3 after 30 min at different conditions, revealing the effects of CO_2 gas and applied current density.

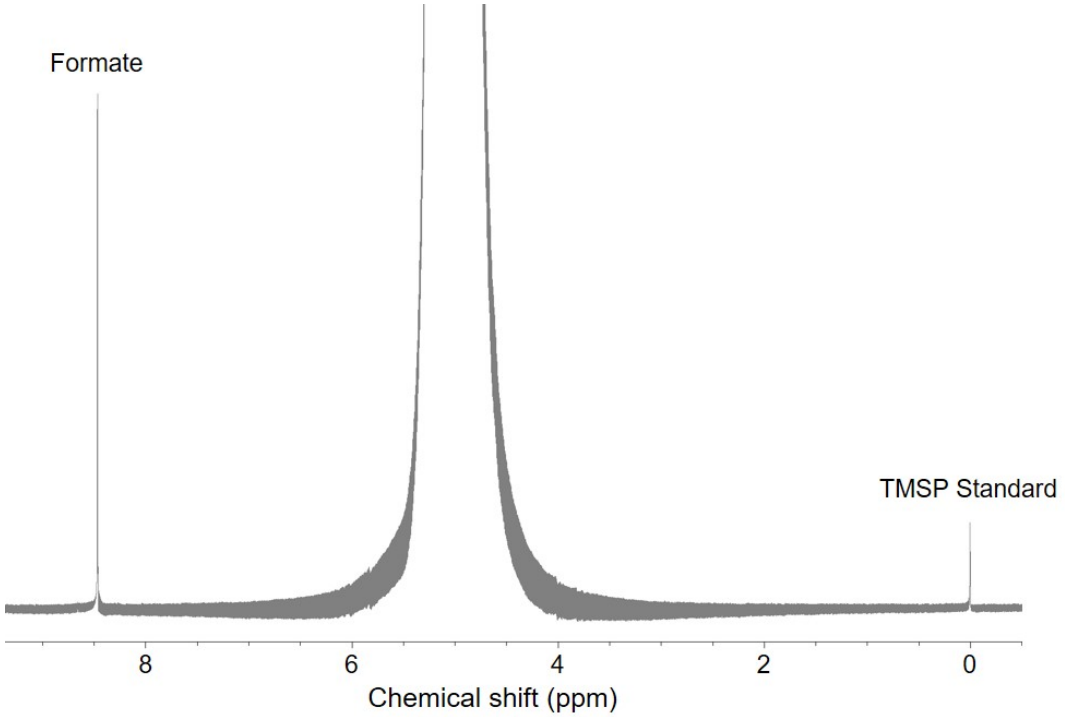

Figure S12 ^{1}H NMR result of liquid product of VS-Bi_2O_3 in 1 M KOH electrolyte after electrolysis at the current density of 200 mA cm^{-2} for 1 h.

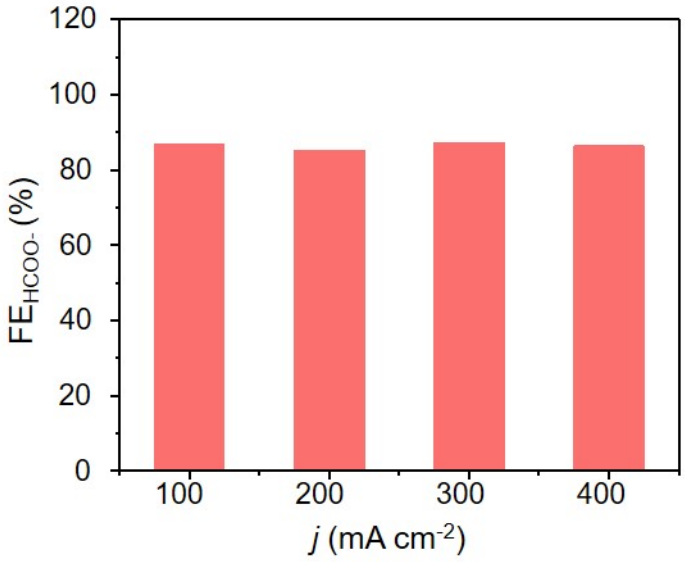

Figure S13 Formate Faradaic efficiency plot of B-Bi_2O_3 at different current densities in 1 M KOH electrolyte in the flow cell system.

Table S2. CO_2RR activity and selectivity comparison of Bi-based catalysts.

Materials	Potential (V vs. RHE, without iR compensation)	FE($HCOO^-$)	Current density (mA cm^{-2})	Cell	Electrolyte	Reference
Bi_2O_3 NS@MCCM	-1.26	93.8	~15	H cell	0.1 M $KHCO_3$	1
f-Bi_2O_3	-1.20	87	25.3	H cell	0.1 M $KHCO_3$	2
Bi NTs	-1.00	~95	24	H cell	0.5 M $KHCO_3$	3
CuBi	-1.00	90	20	H cell	0.5 M $KHCO_3$	4
Bi_2S_3 derived Bi	-0.75	84	5	H cell	0.5 M $NaHCO_3$	5
Bi_2O_3 NTs	-1.05	93	64.5	H cell	0.5 M $KHCO_3$	6
	-0.78	99	~80	Flow cell	1 M $KHCO_3$	
	-0.83	97	~120			
	-0.56	98	~170			
Bi_2O_3@C	-0.90	92	7.5	H cell	0.5 M $KHCO_3$	7
	-1.10	93	~223.7	Flow cell	1 M KOH	
Bi-ene	-0.90	98.6	26.5	H cell	0.5 M $KHCO_3$	8
	-1.10	99.6	26.5	Flow cell	1 M $KHCO_3$	
	-0.57	99.8	100		1 M KOH	
	-0.75	99.2	200			
$BiVO_4$ derived Bi-ene	-1.00	97.4	105.4	Flow cell	1 M $KHCO_3$	9
VS-Bi_2O_3	-1.66	93.7	400	Flow cell	1 M KOH	*This work*

References:

1. S. Liu, X. F. Lu, J. Xiao, X. Wang and X. W. D. Lou, Bi_2O_3 nanosheets grown on multi-channel carbon matrix to catalyze efficient CO_2 electroreduction to HCOOH, *Angew. Chem. Int. Ed.*, 2019, **58**, 13828-13833.

2. T. Tran-Phu, R. Daiyan, Z. Fusco, Z. Ma, R. Amal and A. Tricoli, Nanostructured β-Bi_2O_3 Fractals on Carbon Fibers for Highly Selective CO_2 Electroreduction to Formate, *Adv. Funct. Mater.*, 2019, **30**, 1906478.

3. K. Fan, Y. Jia, Y. Ji, P. Kuang, B. Zhu, X. Liu and J. Yu, Curved surface boosts electrochemical CO_2 reduction to formate via bismuth nanotubes in a wide potential window, *ACS Catal.*, 2019, **10**, 358-364.

4. M. Y. Zu, L. Zhang, C. Wang, L. R. Zheng and H. G. Yang, Copper-modulated bismuth nanocrystals alter the formate formation pathway to achieve highly selective CO_2 electroreduction, *J. Mater. Chem. A*, 2018, **6**, 16804-16809.

5. Y. Zhang, F. Li, X. Zhang, T. Williams, C. D. Easton, A. M. Bond and J. Zhang, Electrochemical reduction of CO_2 on defect-rich Bi derived from Bi_2S_3 with enhanced formate selectivity, *J. Mater. Chem. A*, 2018, **6**, 4714-4720.

6. Q. Gong, P. Ding, M. Xu, X. Zhu, M. Wang, J. Deng, Q. Ma, N. Han, Y. Zhu, J. Lu, Z. Feng, Y. Li, W. Zhou and Y. Li, Structural defects on converted bismuth oxide nanotubes enable highly active electrocatalysis of carbon dioxide reduction, *Nat. Commun.*, 2019, **10**, 2807.

7. P. Deng, F. Yang, Z. Wang, S. Chen, Y. Zhou, S. Zaman and B. Y. Xia, Metal-organic framework-derived carbon nanorods encapsulating bismuth oxides for rapid

and selective CO_2 electroreduction to formate, *Angew. Chem. Int. Ed.*, 2020, **59**, 10807-10813.

8. C. Cao, D. D. Ma, J. F. Gu, X. Xie, G. Zeng, X. Li, S. G. Han, Q. L. Zhu, X. T. Wu and Q. Xu, Metal-organic layers leading to atomically thin bismuthene for efficient carbon dioxide electroreduction to liquid fuel, *Angew. Chem. Int. Ed.*, 2020, **59**, 15014-15020.

9. W. Ma, J. Bu, Z. Liu, C. Yan, Y. Yao, N. Chang, H. Zhang, T. Wang and J. Zhang, Monoclinic scheelite bismuth vanadate derived bismuthene nanosheets with rapid kinetics for electrochemically reducing carbon dioxide to formate, *Adv. Funct. Mater.*, 2020, **31**, 2006704.